Articles

Structure of the Mg^{2+}-Loaded C-Lobe of Cardiac Troponin C Bound to the N-Domain of Cardiac Troponin I: Comparison with the Ca^{2+}-Loaded Structure[†,‡]

Natosha L. Finley, Jack W. Howarth, and Paul R. Rosevear*

Department of Molecular Genetics, Biochemistry, and Microbiology, University of Cincinnati, College of Medicine, 231 Albert Sabin Way, Medical Sciences Building, Cincinnati Ohio 45267-0524

Received February 12, 2004; Revised Manuscript Received July 12, 2004

ABSTRACT: Cardiac troponin C (cTnC) is the Ca^{2+}-binding component of the troponin complex and, as such, is the Ca^{2+}-dependent switch in muscle contraction. This protein consists of two globular lobes, each containing a pair of EF-hand metal-binding sites, connected by a linker. In the N lobe, Ca^{2+}-binding site I is inactive and Ca^{2+}-binding site II is primarily responsible for initiation of muscle contraction. The C lobe contains Ca^{2+}/Mg^{2+}-binding sites III and IV, which bind Mg^{2+} with lower affinity and play a structural as well as a secondary role in modulating the Ca^{2+} signal. To understand the structural consequences of Ca^{2+}/Mg^{2+} exchange in the C lobe, we have determined the NMR solution structure of the Mg^{2+}-loaded C lobe, cTnC(81−161), in a complex with the N domain of cardiac troponin I, cTnI-(33−80), and compared it with a refined Ca^{2+}-loaded structure. The overall tertiary structure of the Mg^{2+}-loaded C lobe is very similar to that of the refined Ca^{2+}-loaded structure as evidenced by the root-mean-square deviation of 0.94 Å for all backbone atoms. While metal-dependent conformational changes are minimal, substitution of Mg^{2+} for Ca^{2+} is characterized by condensation of the C-terminal portion of the metal-binding loops with monodentate Mg^{2+} ligation by the conserved Glu at position 12 and partial closure of the cTnI hydrophobic binding cleft around site IV. Thus, conformational plasticity in the Ca^{2+}/Mg^{2+}-dependent binding loops may represent a mechanism to modulate C-lobe cTnC interactions with the N domain of cTnI.

Muscle contraction is initiated by Ca^{2+} binding to the troponin complex, an assembly of proteins composed of the Ca^{2+}-binding subunit troponin C, (TnC),[1] the inhibitory protein, troponin I (TnI), and the tropomyosin-binding moiety, troponin T (TnT). Calcium binding to the regulatory or N domain of TnC exposes an additional TnI interaction site, which upon binding TnI relieves inhibition of the actomyosin ATPase.

Two isoforms of TnC and TnI are present in striated muscle, slow skeletal or cardiac muscle (cTnC, cTnI), and fast skeletal muscle (sTnC, sTnI). Skeletal and cardiac TnC are highly homologous Ca^{2+}-binding proteins consisting of two globular lobes, each having two EF-hand Ca^{2+}-binding sites, connected by a flexible linker. In the skeletal isoform, the N lobe has two high-specificity but lower affinity Ca^{2+}-binding sites ($K_a \sim 3 \times 10^5$ M^{-1}) (*1*).

The C lobe of both isoforms contains metal-binding sites III and IV that have a high Ca^{2+} affinity ($K_a \sim 2 \times 10^7$ M^{-1}), while also binding Mg^{2+} with lower affinity ($K_a \sim 2 \times 10^3$ M^{-1}) (*1*). Previous studies have shown that Ca^{2+} binding at site III is necessary to maintain a stable C-lobe hydrophobic core (*2*). In addition, site III appears to play a primary role in the affinity of Mg^{2+} for the C lobe (*3*). Both skeletal and cardiac TnC exhibit similar C-lobe Ca^{2+}/Mg^{2+}-dependent interactions with the N domain of TnI (*4*, *5*). The C lobe of cTnC is integrated into the cTnI/cTnT arm in the core cTn structure (*6*). Although the C lobe functions in structural maintenance of the troponin complex, it also plays a role in modulating Ca^{2+}-dependent signaling (*7*−*10*). Serine residues 43 and 45, targets for PKC phosphorylation,

[†] This work is supported by Grant AR44324 from the National Institutes of Health and Training Grant in Cardiovascular Biology HL07382.

[‡] PDB accession code for Mg^{2+}-loaded cTnC(81−161) bound to cTnI(33−80) 1SCV, and PDB accession code for Ca^{2+}-loaded cTnC-(81−161) bound to cTnI(33−80) 1SBJ.

* To whom correspondence should be addressed: Department of Molecular Genetics, Biochemistry, and Microbiology, University of Cincinnati, College of Medicine, Albert Sabin Way, MSB 2105A, Cincinnati, OH 45267. Telephone: (513) 558-3370. Fax: (513) 558-8474. E-mail: paul.rosevear@uc.edu.

[1] Abbreviations: TnC, troponin C; TnI, troponin I; TnT, troponin T; cTnC, recombinant cardiac troponin C (desMet[1]-Ala[2], Cys35Ser); C-cTnC, recombinant cardiac troponin C residues 81−161; sTnC, skeletal TnC; cTnI, cardiac troponin I; N-cTnI, recombinant mouse cardiac troponin I corresponding to residues 33−80 with the N-terminal Met cleaved during expression and purification; cTn, cardiac troponin; DTT, dithiothreitol; PKA, cAMP-dependent protein kinase A; PKC, protein kinase C; EGTA, ethylene glycol-bis(β-aminoethyl ether)-*N*,*N*,*N*′,*N*′-tetraacetic acid; NOESY−HSQC, nuclear Overhauser enhancement spectroscopy; Tris, tris[hydroxymethyl]aminomethane; BCA, bicinchoninic acid; rms, root mean square; RDC, residual dipolar coupling; CSI, chemical-shift index; ASA, accessible surface area; PDB, Protein Data Bank.

10.1021/bi049672i CCC: $27.50
Published on Web 08/20/2004

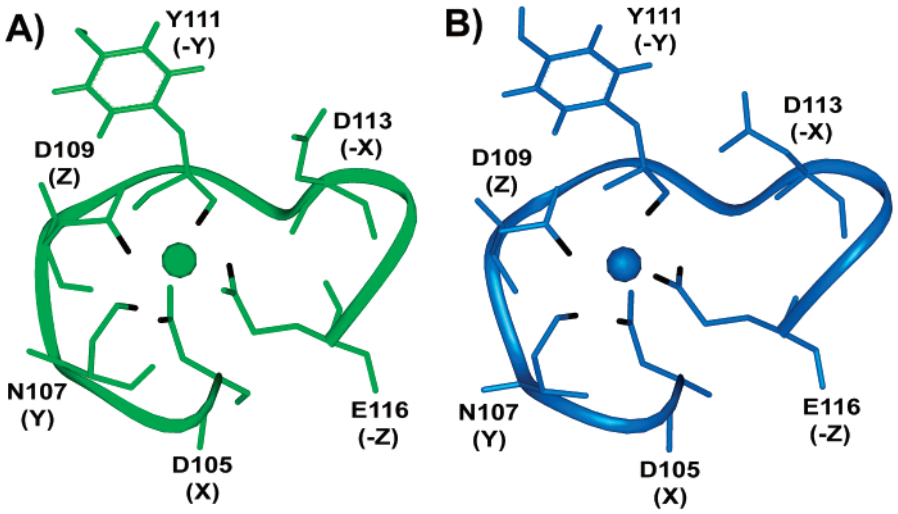

Ligand	1	3	5	7	9	12
Site III	X	Y	Z	-Y	-X	-Z
	D105	N107	D109	Y111	D113	E116
Site IV	X	Y	Z	-Y	-X	-Z
	D141	N143	D145	R147	D149	E152

FIGURE 1: EF-hand Mg^{2+}- and Ca^{2+}-binding loops with the six residues involved in metal coordination numbered. The Mg^{2+}- and Ca^{2+}-loaded C lobes of cTnC are shown in green and blue, respectively. Carboxylate and carbonyl ligand oxygens are colored black. The intervening coordinating water molecule at the $-X$ position is not shown. Coordinating positions (1, 3, 5,7, 9, and 12) within the loop (denoted by *X*, *Y*, *Z*, $-Y$, $-X$, and $-Z$) are given in parentheses next to the residue number. Sequence alignment of Ca^{2+}/Mg^{2+}-binding sites III and IV in the C lobe of cTnC, with the coordinating residues identified, are shown.

lay in the region of cTnI that interacts with the C lobe of cTnC (*5*, *6*, *11*). Phosphorylation at Ser43 and Ser45 by PKC is crucial in cardiac adaptation to hemodynamic stressors such as hypertension and myocardiac infarction (*12*).

The EF-hand or helix−loop−helix motif consists of two flanking helices with an intervening 12-residue loop capable of binding either Ca^{2+} or Mg^{2+} via pentagonal bipyramidal (seven) or octahedral (six) coordination, respectively (*13*−*15*). Calcium is coordinated via oxygen ligands from highly conserved amino acid residues at positions 1(*X*), 3(*Y*), 5(*Z*), 7(−*Y*), 9(−*X*), and 12(−*Z*) (Figure 1). Residues at positions 1(*X*), 3(*Y*), 5(*Z*), 9(−*X*), and 12(−*Z*) provide side-chain oxygens as ligands, whereas residue 7(−*Y*) coordinates the metal ion using its backbone carbonyl oxygen. Residue 9(−*X*) is usually positioned too distant from the coordination sphere to directly bind the metal ion. Instead, a water molecule acts as a bridge for metal ion coordination. Residue 12(−*Z*) is uniquely located in the helix C-terminal to the loop and participates in bidentate coordination of Ca^{2+} by contributing two carboxylate oxygens as ligands.

Strynadka and James were the first to suggest that the residue at position 12 converts from bidentate to monodentate coordination in the presence of Mg^{2+}, permitting the metal-binding loop to collapse around the smaller Mg^{2+} ion (~0.72 Å). This prediction was subsequently confirmed in parvalbumin (*16*). Transmutation from bidentate to monodentate ligation in the presence of Mg^{2+} was the only appreciable structural change detected between Ca^{2+}- and Mg^{2+}-loaded parvalbumin (*16*). Other Mg^{2+} coordination schemes for residues located at position 12 have also been observed (*17*−*19*). However, the physiological relevance of the variations in Mg^{2+} ion coordination by helix−loop−helix motifs remains uncertain.

The C lobe of cTnC contains the Ca^{2+}/Mg^{2+}-dependent cTnC/cTnI interaction site in troponin, making contacts with both cTnI and cTnT. Structural similarity between skeletal and cardiac isoforms of the Ca^{2+}-loaded C lobe bound to TnI suggest a common Ca^{2+}/Mg^{2+}-dependent TnC/TnI interaction site that functions to maintain the integrity of the troponin complex (*4*, *5*). Furthermore, structures of recombinant Ca^{2+}-loaded C lobe are homologous to C-lobe structures in intact Ca^{2+}-loaded TnC, supporting the use of cTnC(81−161) when studying the Ca^{2+}/Mg^{2+}-dependent cTnC/cTnI interaction site in troponin (*4*−*6*, *20*). To date, the three-dimensional structure of Mg^{2+}-loaded cTnC has not been described. We have carried out structural studies of the Mg^{2+}-loaded C lobe of cTnC bound to the N domain of cTnI. The three-dimensional structure of the Mg^{2+}-loaded C lobe provides complimentary information to the structures of the Ca^{2+}-loaded C lobe. This information provides the basis for understanding the structural and functional consequences of Ca^{2+}/Mg^{2+} exchange and the role of the Ca^{2+}/Mg^{2+}-dependent cTnC/cTnI interaction site modulating the Ca^{2+} signal.

MATERIALS AND METHODS

Recombinant Protein Expression and Purification. Isotope-enriched and unlabeled recombinant proteins were expressed, purified, and quantitated as previously described (*5*, *21*). Proteins were determined to be homogeneous by SDS−gel

electrophoresis followed by Coomassie Brilliant Blue staining. Apo[^{15}N,^{13}C]cTnC(81−161) was prepared by dialysis against buffers containing chelating agents (*21*). Subsequently, the apoprotein was dialyzed exhaustively against 20 mM Tris at pH 6.8, 100 mM KCl, 10 mM DTT, 20 mM $MgCl_2$, and 2.0 mM EGTA. Under these conditions, the Mg^{2+}-saturated C lobe could be stored in plastic containers without contamination by residual Ca^{2+} ions for several months. Residual bound Ca^{2+} could be monitored by ^{1}H-^{15}N HSQC spectra of [^{15}N]cTnC(81−161) (*21*).

Complex Formation and Resonance Assignment. Samples of Mg^{2+}-saturated [^{15}N]cTnC(81−161) or [^{13}C,^{15}N]cTnC-(81−161) and unlabeled cTnI(33−80) were combined in equimolar amounts to form stable binary complexes as previously described (*5*). Binary complexes were judged 1:1 by native gel electrophoresis in the presence of 10 mM $MgCl_2$ and by sensitivity-enhanced ^{1}H-^{15}N HSQC spectra (*21*). Samples used for NMR analysis were approximately 1 mM in Mg^{2+}-saturated protein containing 20 mM $Tris_{d11}$ at pH 6.8, 100 mM KCl, 10 mM DTT, 20 mM β-mercaptoethanol, 20 mM $MgCl_2$, 2.0 mM EGTA, and 10% ^2H_2O. Complete EDTA-free protease inhibitor cocktail (Boeringer Mannheim) was used to inhibit any residual protease activity during extensive NMR analysis at 40 °C.

NMR Methodology. Experiments were collected at 40 °C using 500 and 600 MHz Varian Inova spectrometers equipped with pulse-field-gradient units and triple-resonance probes. Backbone and side-chain resonances were assigned from the following suite of NMR experiments as described in Gasmi-Seabrook et al.: (Hβ)CβCα(CO)NH, HNCαCβ, HNCO, HNHA, HNHB, CN−NOESY−HSCQ, H(CCO)-NH, C(CO)NH, and (Hβ)Cβ(CγCδ)Hδ and (Hβ)Cβ-(CγCδCϵ)Hϵ for aromatic residues (*5*). Acquisition parameters for heteronuclear NMR experiments and chemical-shift referencing details can be found in Gasmi-Seabrook et al. (*5*). Values of the $^3J_{HNH\alpha}$ coupling constants were used to estimate φ dihedral angles. Inter-residue NOEs were obtained from ^{15}N-editied NOESY−HSQC and CN−NOESY−HSQC experiments at mixing times of 70 and 150 ms. Felix 2000 was employed to process and analyze NMR data. AngleSearch software was used to estimate χ_1 torsion angles using H_β/H_N ratios of NOE cross-peak intensities (*22*). Residual dipolar couplings were measured by partial alignment of the Ca^{2+}- or Mg^{2+}-loaded complex in the magnetic field using a nonionic liquid-crystalline medium, 5% *n*-dodecyl-penta(ethylene glycol)/*n*-hexanol at a final molar ratio of ∼0.96 and buffer mixture. Couplings between ^{1}H-^{15}N were measured using TROSY-based spin-state-selective experiments (*23*). Residual dipolar couplings were calculated from the difference in measured coupling constants in aqueous isotropic and anisotropic solutions.

Structure Elucidation. The CNS and CNX 1.0 (MSI) software packages were utilized in a multistep protocol to produce an ensemble of solution structures for Mg^{2+}-loaded CcTnC bound to NcTnI. Interproton distances were estimated from NOE cross-peak intensities, measured in ^{15}N-edited NOESY−HSQC and CN−NOESY−HSQC experiments, and used as distance restraints. Measured cross-peak intensities were classified as strong, medium, or weak and used to set distance restraints as previously described (*5*). Sum averaging was utilized for NOEs lacking stereospecifically assigned methylene residues. A total of 500 substructures, in the absence of the Mg^{2+} ion, were generated using distance geometry-simulated annealing (DGSA) and refined as previously described (*5*). During the refinement step, Mg^{2+} was introduced into the structures using modified topology and parameter files in CNS based on ligand distances obtained from Strynadka and James. A set of low-energy structures were further refined using RDCs, using CNX (*24*). A total of 58 ^{1}H-^{15}N RDCs were used to refine the Mg^{2+}-loaded CcTnC structure. NcTnI-bound Ca^{2+}-loaded CcTnC was further refined using a total of 44 ^{1}H-^{15}N RDCs.

Following refinement, 20 low-energy Mg^{2+}- or Ca^{2+}-loaded cTnC(81−161) structures exhibiting no distance restraint violations were selected for further analysis. Structures were evaluated using Procheck−NMR (*25*, *26*) and VADAR (*27*). Coordinates for the final 20 Mg^{2+}-loaded cTnC(81−161) structures bound to cTnI(33−80) and the refined Ca^{2+} -loaded cTnC(81−161) bound to cTnI(33−80) have been deposited in the RCSB Protein Data Bank under the accession codes 1SBJ and 1SCV, respectively. Interhelical angles were measured using interhlx provided by K. Yap from the University of Toronto (Toronto, Canada). The interhelical angle reported by interhlx is $180° - \Theta$, reported by VGM (*28*). Surface areas and volumes were calculated from ensemble average structures for residues 93−159 in Mg^{2+}- and Ca^{2+}-loaded CcTnC bound to NcTnI with VADAR.

RESULTS

Formation of Binary Mg^{2+}-Loaded Structures and NMR Structure Assignment. The apo form of recombinant [^{15}N]-CcTnC was prepared by extensive dialysis against chelating agents (*21*). Formation of the apoprotein was monitored by ^1H_N chemical-shift changes in a series of ^{1}H-^{15}N HSQC spectra. Dialysis of the apoprotein against Mg^{2+} ion yielded Mg^{2+}-loaded [^{15}N]CcTnC. Exchange broadening of ^1H_N resonances belonging to residues in site IV of CcTnC precluded complete resonance assignment and structure determination of the Mg^{2+}-saturated form. The origin of the observed exchange broadening was not pursued further but attributed to weaker Mg^{2+} binding at site IV. The addition of NcTnI to Mg^{2+}-loaded [^{15}N]CcTnC decreased exchange broadening in site IV. Under conditions of the NMR experiments, binding of NcTnI to Mg^{2+}-loaded CcTnC occurs in slow exchange on the NMR time scale, permitting unambiguous resonance assignments for 75 of the 81 CcTnC amide correlations. Backbone resonance assignment for Mg^{2+}-loaded [^{15}N,^{13}C]CcTnC bound to NcTnI relied primarily on (H_β)$C_\beta C_\alpha$(CO)NNH, HN$C_\alpha C_\beta$, and HNCO triple-resonance experiments (*5*, *21*). In a majority of cases, amide resonance assignments could be confirmed by identifying $d_{NN}(i, i+1)$, $d_{NN}(i, i+3)$, and $d_{\alpha N}(i, i+1)$ sequential NOEs obtained from a 70-ms mixing time NOESY−HSQC spectrum. The high-quality NMR spectra permitted nearly complete ^{1}H,^{13}C,^{15}N backbone assignment for residues in CcTnC. Backbone assignments were used as starting points for the side-chain assignment. A suite of 3D heteronuclear experiments, including the TOCSY−HSQC, H(CCO)NH, C(CO)NH, CN−NOESY−HSQC, and NOESY−HSQC, permitted the side-chain assignment of spin systems in Mg^{2+}-loaded [^{15}N,^{13}C]CcTnC bound to NcTnI. Aromatic side-chain assignments were determined using a combination of (H_β)-

$C_\beta(C_\gamma C_\delta)H_\delta$, $(H_\beta)C_\beta(C_\gamma C_\delta C_\epsilon)H_\epsilon$, and CN−NOESY−HSQC experiments.

Magnesium Ligation in CcTnC Bound to NcTnI. Magnesium exchange for Ca^{2+} was accompanied by backbone chemical-shift changes in residues located in metal-binding loops III and IV, with little or no chemical-shift changes in neighboring helices (*21*). The largest chemical-shift changes were observed in ^1H_N resonances of residues occupying positions 3(*Y*), 9(−*X*), and 12 (−*Z*) in sites III and IV (Figure 1). Substitution of Mg^{2+} for Ca^{2+} resulted in deshielding of the ^1H_N at position 3, consistent with a decrease in the hydrogen-bond length between the amide at position 3 and the carboxylate oxygen of Glu at position 12 (*21*). In contrast, the ^1H_N resonance for residues occupying position 9 are shielded, supporting an increase in the hydrogen-bond length between the amide at position 9 and carboxylate oxygen of Glu at position 12 (*21*). Hydrogen-bond-length changes in sites III and IV are consistent with a reorientation of the Glu side-chain carboxylate at position 12 from bidentate coordination, in the presence of bound Ca^{2+}, to mondentate coordination in the presence of bound Mg^{2+}.

The similarity in ^1H_N chemical shifts for Gly at position 6, which hydrogen bonds to the carboxylate oxygen of Asp at position 1 in sites III and IV (*2*), supports a common fold for the N-terminal portion of the metal-binding loops in the presence of Ca^{2+} or Mg^{2+}. Additionally, the amide nitrogen chemical shift of the residue at position 8 has been shown to reflect the metal ligation of the carbonyl oxygen at position 7(−*Y*) (Figure 1) (*29*−*31*). The lack of amide nitrogen chemical-shift changes at position 8, when Mg^{2+} is substituted for Ca^{2+}, is consistent with ligation of Mg^{2+} by the carbonyl oxygen at position 7 in sites III and IV (Figure 1).

Description of the Structures. Mg^{2+}-loaded CcTnC bound to NcTnI contains four helices, spanning residues 93−103 (E), 114−123 (F), 130−139 (G), and 150−156 (H) and two short β strands, residues 111−113 and 147−149, forming an antiparallel β sheet between the two EF-hand metal-binding sites. The overall secondary structure is analogous to that previously determined for Ca^{2+}-loaded CcTnC bound to NcTnI (*5*).

The solution structure was solved using restrained molecular-dynamics-simulated annealing relying on unambiguous NOE-derived distance restraints, ϕ and φ angle restraints, hydrogen-bonding restraints, and RDCs for derivation of geometric restraints (Table 1). Sequential and long-range NOEs were obtained from 70 and 150-ms mixing time NOESY−HSQC spectra and a 150-ms CN−NOESY spectrum. Residual dipolar couplings were acquired by partially aligning the Mg^{2+}-loaded complex in *n*-dodecyl-penta-(ethylene glycol)/*n*-hexanol and buffer. A total of 58 ^1H-^{15}N RDCs were measured in Mg^{2+}-loaded CcTnC bound to NcTnI. Structures were initially calculated in the absence of bound Mg^{2+} ion. During the later stages of structure refinement, four distances were used to coordinate Mg^{2+} in each metal-binding loop. Residues participating in Mg^{2+} coordination were identified by amide proton and nitrogen chemical shifts and later confirmed using RDCs.

Figure 2A shows the best-fit superposition of 20 low-energy Mg^{2+}-loaded CcTnC structures bound to NcTnI. Overall, the helix−loop−helix motifs are well-defined in the Mg^{2+}-saturated state (Figure 3). Superposition of backbone atoms (N, Cα, and C′) for the coordinate-averaged mean structure, determined from the ensemble of 20 low-energy structures, yielded a root-mean-square (rms) deviation of 0.60 Å for defined regions of secondary structure. Residues 81−92 in the N terminus and 159−161 in the C terminus were found to be disordered and are not shown in Figures 2A and 3. The rms deviation from the coordinate-averaged mean structure for all heavy atoms was determined to be 1.25 Å. Table 1 summarizes structural statistics for the final ensemble of structures. No NOE violations greater than 0.18 were detected in any of the accepted structures. The agreement between measured ^1H-^{15}N RDC values and those calculated from the coordinate-averaged mean structure, R^2 of 0.76, support the choice of Mg^{2+} ligation, including monodentate coordination with Glu at position 12. In the coordinate-averaged mean structure, 87% of nonglycine residues lay in the most favorable and 13% in allowed regions of the Ramachandran plot (Table 1). No residues were found to have ψ, ϕ values in the generously allowed or disallowed regions of Ramachandran space (Table 1).

Table 1: Structural Statistics for the Families of 20 Calculated Mg^{2+}- and Ca^{2+}-Loaded CcTnC Structures Bound to NcTnI

	Mg^{2+}-loaded	Ca^{2+}-loaded
distance restraints		
total NOE	814	787
hydrogen bond	4	4
dihedral	78	91
total	896	882
RDC restraints	58	44
CNS energies (kcal/mol)		
E_{total}	57.82	47.82
E_{bond}	1.04	0.79
E_{angle}	32.56	30.85
$E_{improper}$	1.58	1.10
E_{vdw}	10.84	7.74
E_{NOE}	1.75	0.70
E_{cdih}	0.13	0.29
rmsd values[a] (Å)		
backbone	0.68	0.57
helices, β sheets, and Ca^{2+} loops[b]	0.60	0.55
all heavy atoms	1.25	1.16
violations		
distance	0	0
dihedral	0	0
ϕ, ψ values[c]		
most favorable region (%)	87	92
allowed region (%)	13	8

[a] Calculated from the coordinate-averaged mean structure using the family of the 20 lowest energy structures. Values were calculated for residues 94−158. Residues 81−93 and 159−161 are disordered. [b] Values were calculated for residues 94−124 and 130−158. [c] Calculated using PROCHECK.

Our previously published structure of Ca^{2+}-loaded CcTnC bound to NcTnI (*5*) was further refined using ^1H-^{15}N RDCs obtained by partial alignment of the Ca^{2+}-loaded complex in *n*-dodecyl-penta(ethylene glycol)/*n*-hexanol and buffer. Refinement of the Ca^{2+}-loaded structure against 44 RDCs provided an ensemble of 20 low-energy structures that were used to calculate a refined coordinate-averaged mean structure (Figure 2B). Good agreement, R^2 of 0.70, between measured and calculated RDC values was obtained. Superposition of backbone atoms (N, Cα, and C′) for the coordinate-averaged mean structure, determined from the ensemble of 20 low-energy structures, yielded a rms deviation of 0.55 Å for defined regions of the secondary structure. The rms deviation from the coordinate-averaged mean

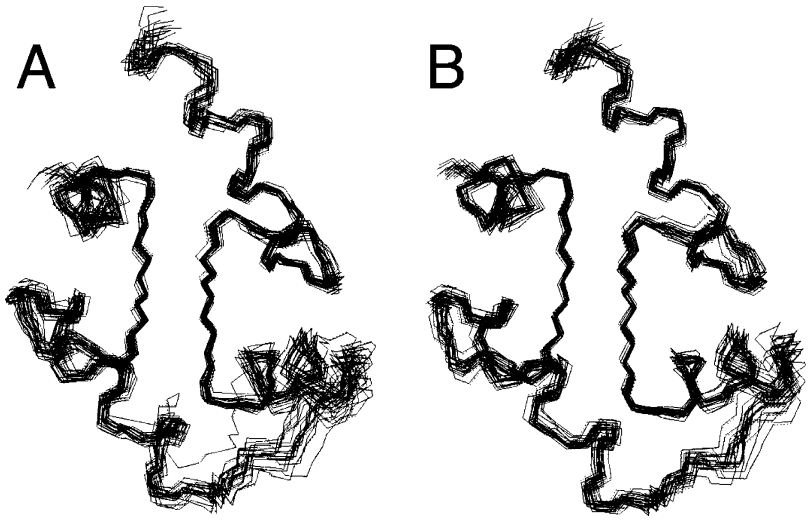

FIGURE 2: Solution structures of Mg^{2+}- and Ca^{2+}-loaded CcTnC bound to NcTnI. Ensembles of the 20 lowest energy structures for Mg^{2+}-loaded CcTnC bound to NcTnI (A) and Ca^{2+}-loaded CcTnC bound to NcTnI (B). Backbone atoms (N, Cα, and C′) of residues 93−158 are shown. Residues 81−92 and 159−161 are disordered.

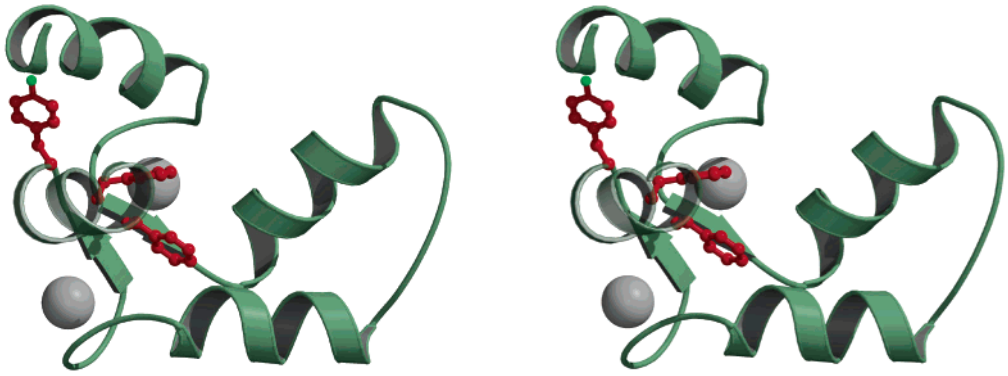

FIGURE 3: Stereoview of NMR-derived solution structure for the Mg^{2+}-loaded C lobe of cTnC bound to the N domain of cTnI. Bound Mg^{2+} ions at sites III and IV are shown as gray spheres. The aromatic side chains of Tyr150, Phe153, and Phe156 in Mg^{2+}-loaded CcTnC bound to NcTnI are shown in red.

structure for all heavy atoms was determined to be 1.16 Å. The coordinate-averaged mean Ca^{2+}-loaded structure had 92% of the nonglycine amino acid residues in the most favorable regions, 8% in allowed regions, and no residues within generously allowed or disallowed regions of the Ramachandran space (Table 1).

Comparison of Experimental Structures. Our new structure of Mg^{2+}-loaded CcTnC bound to NcTnI provides insights into the molecular consequences of Ca^{2+}/Mg^{2+} exchange in troponin and the role of the Ca^{2+}/Mg^{2+}-dependent cTnC/cTnI interaction site in modulating the Ca^{2+} signal (Figure 3). A comparison of the coordinate-averaged mean structures for Ca^{2+}- and Mg^{2+}-loaded CcTnC bound to NcTnI shows homologous polypeptide folds for all defined regions of the secondary structure (Figure 4A). Excluding residues at the flexible termini and in loops, the backbone rms deviation between the two structures is 0.94 Å. Excluding helix H reduces the backbone rms deviation between Ca^{2+}- and Mg^{2+}-loaded forms of the protein to 0.67 Å. The rms deviation increases to 1.87 Å when all backbone residues are used for the superposition.

Total accessible surface areas of 4965, 4982, and 5138 $Å^2$ for free Ca^{2+}-loaded CcTnC, Mg^{2+}-loaded CcTnC/NcTnI, and Ca^{2+}-loaded CcTnC/NcTnI, respectively, were calculated. The increase in total ASA for Ca^{2+}-loaded CcTnC bound to NcTnI, compared to free Ca^{2+}-loaded CcTnC, is attributed to an opening of the C-lobe structure upon binding NcTnI. The total ASA, calculated from ensemble-averaged structures for Mg^{2+}- and Ca^{2+}-loaded CcTnC bound to NcTnI, decreased 156 $Å^2$ in the presence of bound Mg^{2+}. These changes lead to an overall decrease of ~120 $Å^2$ in exposed nonpolar side-chain ASA and a concomitant increase in charged side-chain ASA in the presence of bound Mg^{2+}.

Conformational changes in the helix−loop−helix metal-binding sites were also examined using an interaction-based analysis that calculates a distance difference matrix between each pair of Cα atoms in the Mg^{2+}- and Ca^{2+}-loaded CcTnC structures (*32*). The ensemble-averaged distance difference matrix provides a detailed description of the conformational change taking into account the conformational space occupied by each protein ensemble (*32*, *33*). Using this analysis, the largest conformational change occurs in site IV at the interface between helices G and H (Figure 4B). Substitution with Mg^{2+} results in movement of helix H toward helix G (Figure 4B). Movement of the C-terminal portion of helix H closer to helix G is partially the consequence of Phe153 and Phe156 side-chain reorientation in helix H (Figure 5). The range of χ_1 values for Phe153 and Phe156, where χ_1 is defined as the N−CA−CB−CG, angle, in the ensemble of Ca^{2+}- and Mg^{2+}-loaded forms is less than ±12°. Similarly, the range in χ_2 values for Phe153 and Phe156, where χ_2 is defined as the CA−CB−CG−xD angle, in the ensemble of

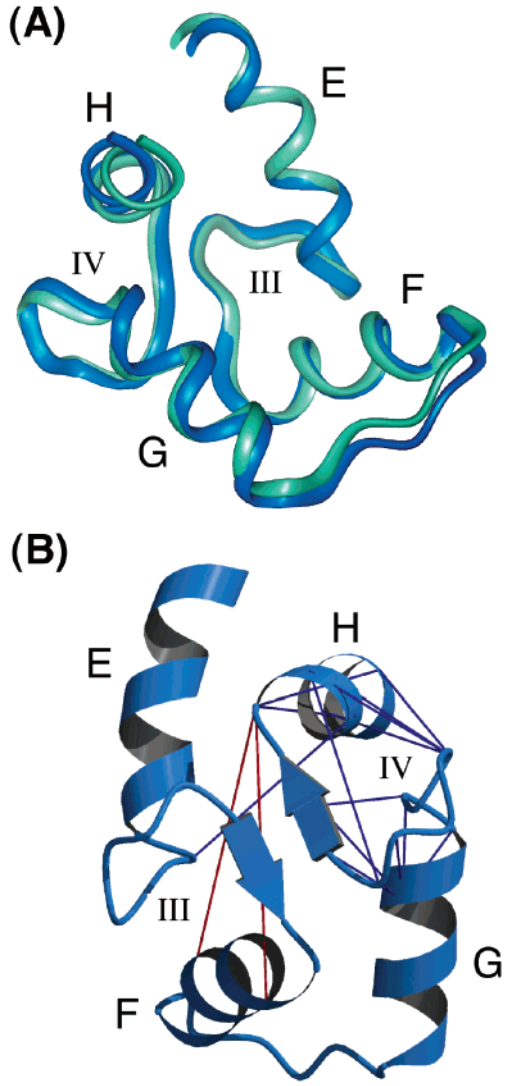

FIGURE 4: Comparison of the solution structures for Mg^{2+}- and Ca^{2+}-loaded CcTnC bound to NcTnI. (A) Ribbon drawing showing the best-fit superposition of ensemble-averaged solution structures for Mg^{2+}- and Ca^{2+}-loaded CcTnC bound to NcTnI. The Mg^{2+}- and Ca^{2+}-loaded C lobes of cTnC are shown in green and blue, respectively. (B) Ensemble-averaged distance difference matrix describing the effect of Ca^{2+} substitution with Mg^{2+} at EF-hand-binding sites III and IV in CcTnC bound to NcTnI. Distance differences in the two metal-loaded forms of CcTnC bound to NcTnI are shown on the ribbon drawing of Ca^{2+}-loaded CcTnC. Distance differences were calculated from the ensemble-averaged distance difference matrix (*33*). Distances that increase with Mg^{2+} substitution are shown in red, and distances that decrease with Mg^{2+} substitution are shown in blue.

Mg^{2+}- and Ca^{2+}-loaded CcTnC structures is less than ±10°. Reorientation of Phe153 and Phe156, as a consequence of Ca^{2+}/Mg^{2+} exchange, may alter both the conformation and the dynamics of the Ca^{2+}/Mg^{2+}-dependent cTn interaction site (parts C and D of Figure 5). Interactions between aromatic side chains < 5 residues apart have been previously shown to effect helix and protein stability (*13*, *34*).

In the Ca^{2+}-loaded complex, helix H comprises a portion of the NcTnI hydrophobic binding cleft (*4*−*6*). Movement of helix H reshapes the hydrophobic surface involved in binding NcTnI, altering the exposed side-chain ASA of Leu97, Leu100, Phe104, Ala108, Tyr111, Ile128, Leu136, Ile148, Tyr150, Leu154, and Phe156 (Figure 6). In addition, in the Mg^{2+}-loaded state, rotation of Tyr150 positions the side-chain hydroxyl to hydrogen bond with the amide of Ser98 and carbonyls of Glu94 and Glu95. These interactions provide a mechanism to transmit site IV conformational changes to helix E and possibly through the linker to the regulatory domain of cTnC.

DISCUSSION

Ca^{2+}/Mg^{2+}-Dependent Troponin Interaction Site. We have prepared the Mg^{2+}-loaded form of the Ca^{2+}/Mg^{2+}-dependent cTn interaction site. The solution structure of Mg^{2+}-loaded CcTnC bound to NcTnI was solved, using isotope-labeling and heteronuclear multidimensional NMR, and compared to a refined Ca^{2+}-loaded structure (Figures 3 and 4). The structure of the Ca^{2+}/Mg^{2+}-dependent cTnC/cTnI interaction site with Mg^{2+} bound has permitted conformational changes induced by Mg^{2+} occupancy of sites III and IV to be investigated. A comparison of Ca^{2+}- and Mg^{2+}-loaded CcTnC structures suggests mechanisms by which Ca^{2+}/Mg^{2+} exchange and PKC phosphorylation of NcTnI could modulate the Ca^{2+} signal. Mobility at the protein−protein interface in Ca^{2+}- and Mg^{2+}-loaded CcTnC/NcTnI, as evidenced by exchange broadening of the amide resonances belonging to NcTnI residues 37−69, precluded structure determination of NcTnI bound in the Ca^{2+}/Mg^{2+}-dependent interaction site. Recently, X-ray crystallography has mapped the Ca^{2+}/Mg^{2+}-dependent interaction site on cTnI to residues 43−79, with residues 43−65 forming an amphiphilic α helix (*6*).

A family of 20 low-energy structures for Mg^{2+}-loaded CcTnC bound to NcTnI had an ensemble backbone rms deviation of 0.60 Å for defined regions of the secondary structure (Figure 2). In the presence of Mg^{2+}, four well-defined helices and a short antiparallel β sheet between EF-hand helix−loop−helix motifs were identified (Figure 3). In addition, the Ca^{2+}-loaded structure, 1FI5, was further refined using 44 ^{1}H-^{15}N RDCs. The backbone rms deviation for the ensemble of refined Ca^{2+}-loaded C-lobe structures bound to NcTnI was 0.55 Å (Figure 2). A best-fit superposition of all backbone atoms of Ca^{2+}- and Mg^{2+}-loaded CcTnC bound to NcTnI gave a low rms deviation of 0.94 Å (Figure 4A). Differences between Ca^{2+}- and Mg^{2+}-loaded C-lobe structures are mainly confined to the C-terminal portion of the metal-binding loops and helix H.

Side-chain reorientations in the C-terminal portion of the metal-binding loops are necessary to accommodate the smaller Mg^{2+} ion. The highly conserved Glu at position 12 was found to change from bidentate coordination with Ca^{2+} to monodentate coordination with Mg^{2+}. Reorientation of Glu at position 12 allows for the collapse of the C-terminal portion of the metal-binding loops about the smaller Mg^{2+} ion. Condensation of the C-terminal portion of metal-binding loop IV pulls helix H toward helix G (Figure 4). A change in the geometry of aromatic−aromatic interactions, in helix H, confers specificity to the positioning of helix H with respect to the remaining C-lobe structure. This results in a Mg^{2+}-loaded structure that is slightly more closed than observed in the presence of Ca^{2+} but more open than observed for free Ca^{2+}-loaded CcTnC. Movement of helix H in response to condensation of the C-terminal portion of loop IV to accommodate the smaller Mg^{2+} ion may explain the apparent weaker affinity of Mg^{2+} and the exchange broadening of resonances belonging to residues in site IV

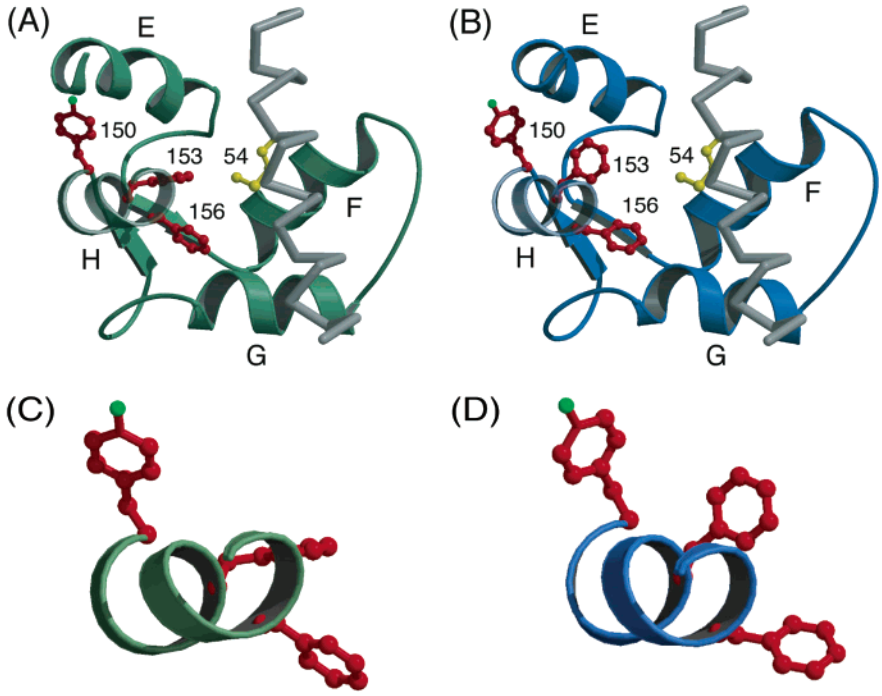

FIGURE 5: Ribbon drawings showing structures of Mg^{2+}- and Ca^{2+}-loaded CcTnC bound to NcTnI. (A) Mg^{2+}-loaded CcTnC bound to NcTnI. (B) Ca^{2+}-loaded CcTnC bound to NcTnI. (C) Ribbon drawing of helix H in the ensemble-averaged Mg^{2+}-loaded CcTnC structure showing positions of aromatic side-chains Tyr150, Phe153, and Phe156. (D) Ribbon drawing of helix H in the ensemble-averaged Ca^{2+}-loaded CcTnC structure showing positions of aromatic side-chains Tyr150, Phe153, and Phe156. The Mg^{2+}- and Ca^{2+}-loaded C lobes of cTnC are shown in green and blue, respectively. Aromatic side chains of Tyr150, Phe153, and Phe156 are shown in red. The N domain of cTnI, shown in gray, was modeled onto the Mg^{2+}- and Ca^{2+}-loaded structures (A and B). Methionine 54 in cTnI is shown in yellow. The NcTnI peptide was modeled using the structure of sTnC bound to sTnI(1−47) (PDB accession code 1A2X) (*4*).

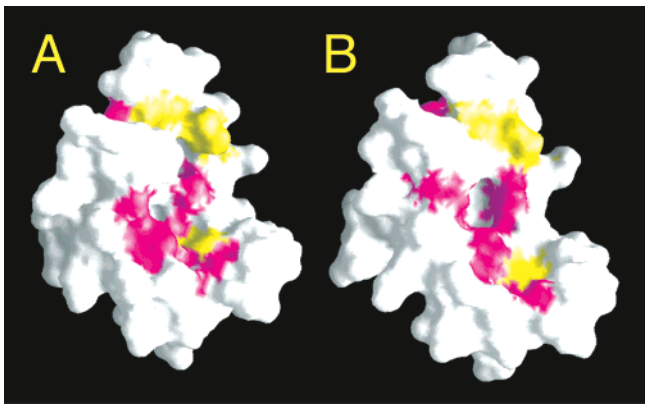

FIGURE 6: Molecular surfaces of the Mg^{2+}- and Ca^{2+}-loaded C lobes of cTnC bound to NcTnI showing the side chains of nonpolar residues that undergo a change in side-chain ASA during Ca^{2+}/Mg^{2+} exchange. Molecular surfaces showing hydrophobic residues located in the NcTnI hydrophobic binding crevice of Mg^{2+}-loaded CcTnC bound to NcTnI (A) and Ca^{2+}-loaded CcTnC bound to NcTnI (B). Surface residues are white with the side chains of nonpolar residues experiencing a decrease in exposed side-chain ASA in going from Ca^{2+} bound at sites III and IV to Mg^{2+} bound in CcTnC shown in purple. Nonpolar residues experiencing an increase in exposed side-chain ASA in going from Ca^{2+} to Mg^{2+} bound are shown in yellow. Molecular surfaces were calculated using GRASP.

Table 2: Comparison of Interhelical Angles and Distances for Ca^{2+}- and Mg^{2+}-Loaded CcTnC in the Presence and Absence of NcTnI

	Interhelical Angles (deg)[a]		
helix pair	CcTnC[b] Ca^{2+}-loaded	CcTnC/NcTnI[c] Mg^{2+}-loaded	CcTnC/NcTnI[c] Ca^{2+}-loaded
E/F	101 ± 8	90 ± 4	96 ± 4
G/H	113 ± 7	107 ± 5	94 ± 3
	Interhelical Distances (Å)[a]		
helix pair	CcTnC[b] Ca^{2+}-loaded	CcTnC/NcTnI[c] Mg^{2+}-loaded	CcTnC/NcTnI[c] Ca^{2+}-loaded
E/F	16.4 ± 0.4	17.9 ± 0.5	17.7 ± 0.4
G/H	15.3 ± 0.4	15.1 ± 0.3	16.0 ± 0.2

[a] Interhelical angles and distances were calculated using interhlx, as described in the Materials and Methods, from the coordinate-averaged mean structure using the family of the 20 lowest energy structures. [b] Calculated using the ensemble-averaged Ca^{2+}-loaded CcTnC structure (PDB accession code 1SCV). [c] Calculated using the refined ensemble-averaged Ca^{2+}-loaded CcTnC/NcTnI structure (PDB accession code 1SCV) and the refined ensemble-averaged Mg^{2+}-loaded CcTnC/NcTnI structure (PDB accession code 1SBJ).

in the absence of NcTnI. Thus, plasticity in the C-terminal portion of the metal-binding loops seems to permit discrimination between Ca^{2+} and Mg^{2+} ions and may modulate the Ca^{2+} signal through the Ca^{2+}/Mg^{2+}-dependent interaction site.

Molecular Basis of Ca^{2+}/Mg^{2+} Exchange. Structural responses to Ca^{2+}- and Mg^{2+}-binding can be more quantitatively analyzed by comparison of interhelical angles. Calculation of interhelical angles, the angle between helix pairs, provides a measure of the degree of opening or hydrophobic cleft exposure in EF-hand proteins (*28*, *31*). A small interhelical angle defines a more open conformation, whereas a larger interhelical angle defines a more closed conformation in which the hydrophobic crevice is less exposed to the solvent. Interhelical angles for Ca^{2+}- and Mg^{2+}-loaded CcTnC bound to NcTnI are consistent with both metal-bound forms having a more open/exposed hydrophobic cleft than free Ca^{2+}-loaded CcTnC (Table 2). The E/F interhelical angle and distance describing Ca^{2+}/Mg^{2+}-binding site III, calculated from the ensemble-averaged structure,

were found to be similar in both the Mg^{2+}- and Ca^{2+}-loaded states (Table 2). However, the G/H interhelical angle, describing Ca^{2+}/Mg^{2+}-binding site IV, was found to change appreciably in the Mg^{2+}-loaded structure. Substitution of Mg^{2+} by Ca^{2+} at site IV increases the G/H interhelical angle by ~13° and decreases the interhelical distance by ~1.1 Å (Table 2). Changes observed in the G/H interhelical angle and distance are consistent with condensation of the C-terminal portion of site IV around the smaller Mg^{2+} ion, dragging helix H toward helix G resulting in a more closed Mg^{2+}-loaded structure. The G/H interhelical distance, 15.1 Å, in Mg^{2+}-loaded CcTnC bound to NcTnI is most similar to the interhelical distance, 15.3 Å, observed in the free Ca^{2+}-loaded C lobe (Table 2). In free Ca^{2+}-loaded CcTnC, the hydrophobic crevice is less exposed (*5*). Thus, Mg^{2+} -induced conformational changes at site IV may provide a mechanism for modulating the Ca^{2+} signal through C-lobe interactions with the IT arm of cTn. The IT arm, a rigid coil-coiled subdomain composed of cTnI and cTnT, is suggested to play a central role in the regulation of muscle contractions because it resides near both the tropomyosin-binding site on cTnT and the regulatory region of cTnI (*6*).

Modulating NcTnI Binding. Partial closure of the hydrophobic pocket is expected to alter the ability of the conserved Met in TnI and Met54 in NcTnI to completely insert into the hydrophobic pocket, reducing the entropic component observed for complex formation in the presence of Mg^{2+}. Methionine 21 in sTnI, homologous to Met54 in cTnI, is thought to play a central role in the Ca^{2+}/Mg^{2+}-dependent interaction in skeletal Tn through multiple van der Waal interactions with residues in helix H, Phe151, Met154, and Met155 (*4*). On the basis of structural homology of the Ca^{2+}/Mg^{2+}-dependent interaction sites in cardiac and skeletal TnC isoforms (*5*), Met54 in NcTnI would interact with Phe153, Phe156, and Met157 in helix H of cTnC. All three residues undergo a significant Mg^{2+}-induced conformational change (Figure 5).

Thermodynamic studies suggest that in the presence of Ca^{2+}, hydrophobic forces dominate the cTnC C-lobe interaction with cTnI (*9*). Substitution of Ca^{2+} by Mg^{2+} is characterized by a decrease in K_a with increasing ionic strength, suggesting that electrostatic interactions contribute significantly to the stability of the CcTnC/cTnI complex in the presence of Mg^{2+} (*9*). This is likely the consequence of cTnI being unable to fully insert into the C-lobe hydrophobic crevice and the altered side-chain ASA of charged residues adjacent to the hydrophobic crevice (Figure 6). In addition, conformational changes in aromatic−aromatic interactions may alter the structural stability and protein−protein interactions. Thus, subtle changes in side-chain conformations or dynamics could be used to fine-tune or modulate Ca^{2+}/Mg^{2+}-dependent interactions. We have previously noted significant mobility at the protein−protein interface in Ca^{2+}-loaded CcTnC/NcTnI (*5*). Similar mobility in the hydrophobic core of parvalbumin has been observed (*30*). Specifically, rates of Phe rotamer interconversion have been suggested to be dependent on the nature of the bound cation (*35*). A mobile hydrophobic core may facilitate conformational rearrangements necessary to accommodate the smaller Mg^{2+} ion and regulate Ca^{2+}/Mg^{2+} exchange without the loss of the CcTnC/NcTnI interaction.

In Summary. We have determined high-resolution solution structures for the C lobe of cTnC bound to the N domain of cTnI in the presence of bound Mg^{2+} or Ca^{2+} ions. The solution structures of Mg^{2+}-loaded CcTnC bound to NcTnI represent the first Mg^{2+}-loaded TnC structure. The overall tertiary structure of Mg^{2+}-loaded CcTnC is very similar to that of the refined Ca^{2+}-loaded structure as evidenced by rms deviations of 0.94 and 1.34 Å for all backbone and heavy atoms, respectively. While metal-dependent backbone conformational changes in the C lobe of cTnC are minimal, conformational plasticity within the Ca^{2+}/Mg^{2+}-dependent cTnC/cTnI interaction site permits condensation of the C-terminal portion of metal-binding sites III and IV, leading to the closure of the hydrophobic pocket around site IV. Thus, mobility within the hydrophobic core could be intimately linked to the role of the C lobe in the modulation of the Ca^{2+} signal. The availability of both Ca^{2+}- and Mg^{2+}-loaded C-lobe cTnC structures bound to NcTnI is an essential first step in understanding thermodynamic and kinetic properties of protein−cation and protein−protein interactions governing the Ca^{2+}/Mg^{2+}-dependent interaction site. While controversy still exits regarding the physiological relevance of Ca^{2+}/Mg^{2+} exchange in troponin, this study highlights both similarities and differences between Ca^{2+} and Mg^{2+}-loaded C-lobe cTnC structures. In addition, these structures provide a molecular stage on which to interpret the molecular mechanism by which PKC phosphorylation at serines 43 and 45 of cTnI modulates the Ca^{2+} signal.

ACKNOWLEDGMENT

We especially thank James J. Chou and Ad Bax for the protocol used in structural refinement against residual dipolar couplings and helpful discussions, as well as Perttu Permi and Arto Annila for spin-state-selective TROSY pulse sequences used in measuring residual dipolar couplings. We are grateful to Lewis Kay for providing the pulse sequences and to Walter Chazin for the program analyzing the ensemble-averaged distance difference matrix. We especially thank Ian Trayer for access to unpublished data and for useful discussions.

REFERENCES

1. Potter, J. D., and Gergely, J. (1975) The calcium and magnesium binding sites on troponin and their role in the regulation of myofibrillar adenosine triphosphatase, *J. Biol. Chem. 250*, 4628−4633.
2. Brito, R. M., Krudy, G. A., Negele, J. C., Putkey, J. A., and Rosevear, P. R. (1993) Calcium plays distinctive structural roles in the N- and C-terminal domains of cardiac troponin C, *J. Biol. Chem. 268*, 20966−20973.
3. Wang, S., George, S. E., Davis, J. P., and Johnson, J. D. (1998) Structural determinants of Ca^{2+} exchange and affinity in the C terminal of cardiac troponin C, *Biochemistry 37*, 14539−14544.
4. Vassylyev, D. G., Takeda, S., Wakatsuki, S., Maeda, K., and Maeda, Y. (1998) Crystal structure of troponin C in complex with troponin I fragment at 2.3 Å resolution, *Proc. Natl. Acad. Sci. U.S.A. 95*, 4847−4852.
5. Gasmi-Seabrook, G. M., Howarth, J. W., Finley, N., Abusamhadneh, E., Gaponenko, V., Brito, R. M., Solaro, R. J., and Rosevear, P. R. (1999) Solution structures of the C-terminal domain of cardiac troponin C free and bound to the N-terminal domain of cardiac troponin I, *Biochemistry 38*, 8313−8322.
6. Takeda, S., Yamashita, A., Maeda, K., and Maeda, Y. (2003) Structure of the core domain of human cardiac troponin in the Ca^{2+}-saturated form, *Nature 424*, 35−41.

7. Burkart, E. M., Sumandea, M. P., Kobayashi, T., Nili, M., Martin, A. F., Homsher, E., and Solaro, R. J. (2003) Phosphorylation or glutamic acid substitution at protein kinase C sites on cardiac troponin I differentially depress myofilament tension and shortening velocity, *J. Biol. Chem. 278*, 11265−11271.
8. Burkart, E. M., Arteaga, G. M., Sumandea, M. P., Prabhakar, R., Wieczorek, D. F., and Solaro, R. J. (2003) Altered signaling surrounding the C-lobe of cardiac troponin C in myofilaments containing an α-tropomyosin mutation linked to familial hypertrophic cardiomyopathy, *J. Mol. Cell. Cardiol. 35*, 1285−1293.
9. Calvert, M. J., Ward, D. G., Trayer, H. R., and Trayer, I. P. (2000) The importance of the carboxyl-terminal domain of cardiac troponin C in Ca^{2+}-sensitive muscle regulation, *J. Biol. Chem. 275*, 32508−32515.
10. Pi, Y.-Q., Zhang, D., Kemnitz, K. R., Wang, H., and Walker, J. W. (2003) Protein kinase C and A sites on troponin I regulate myofilament Ca^{2+} sensitivity and ATPase activity in the mouse myocardium, *J. Physiol. 552*, 845−857.
11. Krudy, G. A., Kleerekoper, Q., Guo, X., Howarth, J. W., Solaro, R. J., and Rosevear, P. R. (1994) NMR studies delineating spatial relationships within the cardiac troponin I-troponin C complex, *J. Biol. Chem. 269*, 23731−23735.
12. Montgomery, D. E., Wolska, B. M., Pyle, W. G., Roman, B. B., Dowell, J. C., Buttrick, P. M., Koretsky, A. P., Del Nido, P., and Solaro, R. J. (2002) α-Adrenergic response and myofilament activity in mouse hearts lacking PKC phosphorylation sites on cardiac TnI, *Am. J. Physiol. Heart Circ. Physiol. 282*, H2397−H2405.
13. Burley, S. K., and Petsko, G. A. (1985) Aromaitc−aromatic interaction: A mechanism of protein structure stabilization, *Science 229*, 23−28.
14. Kretsinger, R. H., and Nockolds, C. E. (1973) Carp Muscle Calcium-binding Protein. II. Structure determination and general description, *J. Biol. Chem. 248*, 3313−3326.
15. Falke, J. J., Drake, S. K., Hazard, A. L., and Peersen, O. B. (1994) *Q. Rev. Biophys. 27*, 219−290.
16. Declercq, J. P., Tinant, B., Parello, J., and Rambaud, J. (1991) Ionic interactions with parvalbumins. Crystal structure determination of pike 4.10 parvalbumin in four different ionic environments, *J. Mol. Biol. 220*, 1017−1039.
17. Yumoto, F., Nara, M., Kagi, H., Iwasaki, W., Ojima, T., Nishita, K., Nagata, K., and Tanokura, M. (2001) Coordination structures of Ca^{2+} and Mg^{2+} in Akazara scallop troponin C in solution. FTIR spectroscopy of side-chain COO^- groups, *Eur. J. Biochem. 268*, 6284−6290.
18. Malmendal, A., Evenas, J., Thulin, E., Gippert, G. P., Drakenberg, T., and Forsen, S. (1998) When size is important. Accommodation of magnesium in a calcium binding regulatory domain, *J. Biol. Chem. 273*, 28994−29001.
19. Andersson, M., Malmendal, A., Linse, S., Ivarsson, I., Forsen, S., and Svensson, L. A. (1997) Structural basis for the negative allostery between Ca^{2+}- and Mg^{2+}-binding in the intracellular Ca^{2+}-receptor calbindin D(9k), *Protein Sci. 6*, 1139−1147.
20. Dvoretsky, A., Abusamhadneh, E. M., Howarth, J. W., and Rosevear, P. R. (2002) Solution structure of calcium-saturated cardiac troponin C bound to cardiac troponin I, *J. Biol. Chem. 277*, 38565−38570.
21. Finley, N., Dvoretsky, A., and Rosevear, P. R. (2000) Magnesium−calcium exchange in cardiac troponin C bound to cardiac troponin I, *J. Mol. Cell. Cardiol. 32*, 1439−1446.
22. Polshakov, V. I., Frenkiel, T. A., Westley, B., Chadwick, M., May, F., Carr, M. D., and Feeney, J. (1995) NMR-based structural studies of the pNR-2/pS2 single domain trefoil peptide. Similarities to porcine spasmolytic peptide and evidence for a monomeric structure, *Eur. J. Biochem. 233*.
23. Permi, P., Heikkinen, S., Kilpelainen, I., and Annila, A. (2000) Measurement of (1)J(NC′) and (2)J(H(N))(C′) couplings from spin-state-selective two-dimensional correlation spectrum, *J. Magn. Reson. 140*, 32−40.
24. Chou, J. J., Delaglio, F., and Bax, A. (2000) Measurement of one-bond ^{15}N-$^{13}C'$ dipolar couplings in medium sized proteins, *J. Biomol. NMR 18*, 101−105.
25. Laskowski, R. A., MacArthur, M. W., Moss, D. S., and Thornton, J. M. (1993) Procheck: A program to check the stereochemical quality of protein structures, *J. Appl. Crystallogr. 26*, 283−291.
26. Laskowski, R. A., Rullmannn, J. A., MacArthur, M. W., Kaptein, R., and Thornton, J. M. (1996) AQUA and PROCHECK−NMR: Programs for checking the quality of protein structures solved by NMR, *J. Biomol. NMR 8*, 477−486.
27. Willard, L., Ranjan, A., Zhang, H., Monzavi, H., Boyko, R. F., Sykes, B. D., and Wishart, D. S. (2003) VADAR: A web server for quantitative evaluation of protein structure quality, *Nucleic Acids Res. 31*, 3316−3319.
28. Yap, K. L., Ames, J. B., Swindells, M. B., and Ikura, M. (2002) Vector geometry mapping. A method to characterize the conformation of helix−loop−helix calcium-binding proteins, *Methods Mol. Biol. 173*, 317−324.
29. Biekofsky, R. R., Martin, S. R., Browne, J. P., Bayley, P. M., and Feeney, J. (1998) Ca^{2+} coordination to backbone carbonyl oxygen atoms in calmodulin and other EF-hand proteins: ^{15}N chemical shifts as probes for monitoring individual-site Ca^{2+} coordination, *Biochemistry 37*, 7617−7629.
30. Baldellon, C., Padilla, A., and Cave, A. (1992) Kinetics of amide proton exchange in parvalbumin studied by ^1H 2D NMR. A comparison of the calcium and magnesium loaded forms, *Biochimie 74*, 837−844.
31. Ikura, M., Clore, G. M., Gronenborn, A. M., Zhu, G., Klee, C. B., and Bax, A. (1992) Solution structure of a calmodulin-target peptide complex by multidimensional NMR, *Science 256*, 632−638.
32. Nelson, M. R., and Chazin, W. J. (1998) An interaction-based analysis of calcium-induced conformational changes in Ca^{2+} sensor proteins, *Protein Sci. 7*, 270−282.
33. Akke, M., Forsen, S., and Chazin, W. J. (1995) Solution structure of (Cd^{2+})1-calbindin D 9k reveals details of the stepwise structural changes along the Apo*rarr;(Ca^{2+}) 1II *rarr;(Ca^{2+})2I,II binding pathway, *J. Mol. Biol. 252*, 102−121.
34. Bhattacharyya, R., Samanta, U., and Chakrabarti, P. (2002) Aromatic−aromatic interactions in and around helices, *Protein Eng. 15*, 91−100.
35. Zanotti, J. M., Bellissent-Funel, M. C., and Parello, J. (1999) Hydration-coupled dynamics in proteins studied by neutron scattering and NMR: The case of the typical EF-hand calcium-binding parvalbumin, *Biophys. J. 76*, 2390−2411.

BI049672I